Experimental redox transformations of uranium phosphate minerals and mononuclear species in a contaminated wetland

Lucie Stetten, Pierre Lefebvre, Pierre Le Pape, Arnaud Mangeret, Pascale Blanchart, Pauline Merrot, Jessica Brest, Anthony Julien, John R Bargar, Charlotte Cazala, et al.

Experimental redox transformations of uranium phosphate minerals and mononuclear species in a contaminated wetland

Lucie Stetten[1,2,3]*, Pierre Lefebvre[1], Pierre Le Pape[1], Arnaud Mangeret[2], Pascale Blanchart[2], Pauline Merrot[1], Jessica Brest[1], Anthony Julien[2], John R. Bargar[4], Charlotte Cazala[2], Guillaume Morin[1]

[1] Institut de Minéralogie, de Physique des Matériaux et de Cosmochimie (IMPMC), UMR 7590 CNRS-Sorbonne Université-IRD-MNHN, case 115, 4 place Jussieu, 75252 Paris Cedex 5, France

[2] Institut de Radioprotection et de Sûreté Nucléaire, IRSN, 31 avenue de la Division Leclerc, 92262 Fontenay-aux-Roses, France

[3] University of Vienna, Centre for Microbiology and Environmental Systems Science, Department of Environmental Geosciences, Althanstraße 14, UZA II, 1090 Vienna, Austria

[4] Stanford Synchrotron Radiation Lightsource (SSRL), SLAC National Accelerator National Laboratory, MS 69, 2575 Sand Hill Road, Menlo Park, CA 94025, USA

*luciestetten@gmail.com

Revised version to be submitted to *Journal of hazardous materials*

GRAPHICAL ABSTRACT

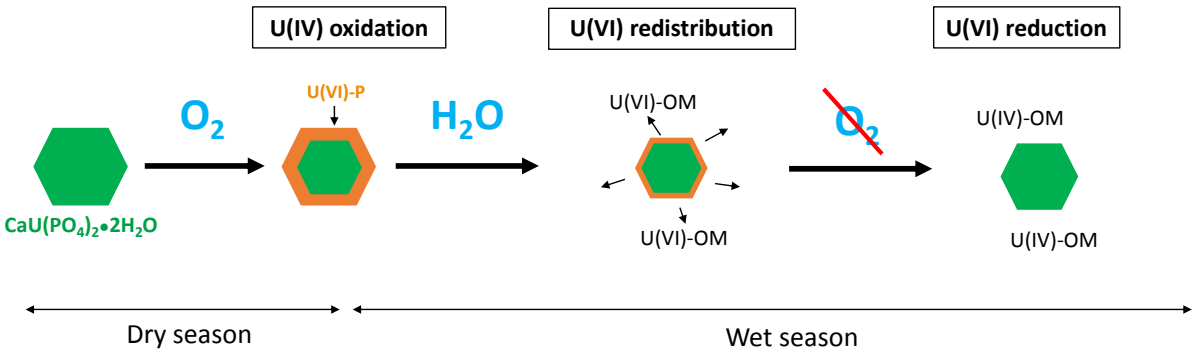

ABSTRACT

Reducing conditions and high organic carbon content make wetlands favorable to uranium (U) sequestration. However, such environments are subjected to water-table fluctuations that could impact the redox behavior of U and its mobility. Our previous study on U speciation in a highly contaminated wetland has suggested a major role of water-table redox fluctuations in the redistribution of U from U(IV)-phosphate minerals to organic U(VI) and U(IV) mononuclear species. Here, we investigate the mechanisms of these putative processes by mimicking drying or flooding periods *via* laboratory incubations of wetland samples. LCF-XANES and EXAFS analyses show the total oxidation/reduction of U(IV)/U(VI)-mononuclear species after 20 days of oxic/anoxic incubation, whereas U-phosphate minerals appear to be partly oxidized/reduced. SEM-EDXS combined with µ-XRF and µ-XANES analyses suggest that autunite $Ca(UO_2)_2(PO_4)_2 \bullet 11H_2O$ is reduced into lermontovite $U(PO_4)(OH) \bullet H_2O$, whereas oxidized ningyoite $CaU(PO_4)_2 \bullet 2H_2O$ is locally dissolved. The release of U from this latter process is observed to be limited by U(VI) adsorption to the surrounding soil matrix and further re-reduction into mononuclear U(IV) upon anoxic cycling. Analysis of incubation waters show, however, that dissolved organic carbon enhances U solubilization even under anoxic conditions. This study brings important information that help to assess the long-term stability of U in seasonally saturated organic-rich contaminated environments.

Keywords: wetland, uranium, redox transformations, soil incubation, X-ray absorption spectroscopy

1. INTRODUCTION

Uranium is a toxic element [1] that naturally occurs in the continental crust at an average concentration of 2.7 $mg.kg^{-1}$ [2]. It locally concentrates in economic deposits *via* reductive precipitation and/or hydrothermal processes [3] and has been mined for decades in several countries worldwide. Uranium mining operations and legacies have been shown to be responsible for local increases of U contaminations in surrounding surface environments. For instance, U concentrations exceeding the geochemical background were found in aquifer sediments [4], lacustrine sediments [5], soils [6] and wetlands [7-10] in the vicinity of former U mining sites.

Organic-rich wetlands are favorable to develop reducing conditions and have been recognized to accumulate uranium both *via* organic complexation of U(VI) and U(VI) reduction to less soluble U(IV) species. These environments are thus considered as being able to naturally attenuate U migration from nearby mining sites [7,10]. However, the long-term fate of U in wetlands remains unclear, especially when they exhibit intermittent oxidizing conditions due to water-table fluctuations [10]. Indeed, non-crystalline U species that have been identified as major U species in wetlands, such as mononuclear U(VI) and U(IV) complexes bound to organic matter [10,11-13], are known to be potentially mobile under both oxic [14-17] and anoxic conditions [7,18]. In addition, U(IV)-phosphate minerals may also play an important role in U retention in mining-contaminated wetlands. Indeed, such phases have been recently recognized as important U hosts in contaminated environments [10,19] and as possible products of microbial U(VI) reduction [16,20-21]. However, the geochemical reactivity of these phases when submitted to redox fluctuations is still scarcely documented and remains debated. For instance, Latta et al. (2016) [22] reported that the oxidation of a

synthetic amorphous U(IV)-phosphate resulted in the formation of a low-solubility U(VI)–phosphate phase. In contrast, oxidation of a ningyoite-like mineral (ideal formula $CaU(PO_4)_2•2H_2O$) has been shown to lead to significant U remobilization [16]. To this regard, the reactivity of U(IV)-phosphate minerals such as ningyoite needs to be further investigated. In this context, our recent study of U speciation in a highly contaminated wetland in Brittany, France [10] has suggested that low water-table level conditions can lead to oxidative dissolution of U(IV)-phosphate minerals, especially ningyoite, and to subsequent sorption of U(VI) to soil organic matter, while flooding conditions could favor further reduction of U(VI) to U(IV) organic complexes. Based on these findings, the present study aims at elucidating the micro- and molecular-scale mechanisms underlying such U redistribution processes, by performing incubations experiments that mimics typical redox changes induced by water-table fluctuations in a seasonally saturated wetland.

2. MATERIALS & METHODS

2. 1. Wetland soil samples

The wetland soil samples selected for the present incubation experiments were collected in the highly contaminated wetland previously studied by Stetten et al. (2018b) [10], located near the former U-mine Ty Gallen in Brittany, France. Four types of soil layers were distinguished: a humus layer almost devoid of crystalline mineral components (O-type), organic-rich or organic-poor soil layers (A_1- and A_2-type layers respectively), and mine water deposit layers inherited from former mining operations (Figure SI-1b) [10].

For oxic incubations, three pristine reduced soil samples were selected below the water-table (Figure 1): an organo-mineral soil sample from a A_2-type layer (C2-25 cm sample) and two

125 samples from mine water deposit layers (C2-30 cm and C6-33 cm samples). These samples
126 were obtained from the C2 and C6 soil cores that were collected, vacuum-dried in a desiccator
127 to a vacuum limit of 0.5 mbar and preserved under anoxic conditions [10].
128 For anoxic incubations, a humus layer sample (S1 sample; Figure 2) and a mine water deposit
129 layer sample (S2 sample) were collected with a spade in the wetland in November 2015 and
130 were stored under aerobic conditions at ambient temperature (21 °C), before the incubation
131 experiments. These two latter samples were considered as representative of wetland soil
132 samples exposed to a prolonged period of dryness and were thus used as starting samples for
133 anoxic incubation experiments. In addition, a pristine organic-rich soil sample from the C2
134 core corresponding to the A_1-type layer above the water-table level (C2-5 cm sample) was
135 also used as starting sample for anoxic incubation.
136
137 **2. 2. Incubation experiments**
138
139 For oxic incubation experiments, ~300 mg of dry soil was supplemented with ~1 ml of O_2-
140 free milli-Q water and were put in 50 ml tinted glass vials. The glass vials were then left open
141 to air on a lab bench during 20 days in order to simulate a period of dryness. As these pristine
142 soil samples exhibit similar uranium speciation [10], they were used as triplicates for this
143 experiment (C2-25cm_oxic; C2-30cm_oxic; C6-33cm_oxic). Anoxic incubation experiments
144 were conducted in an anaerobic glove box (O_2 < 20 ppm vol. in N_2) at IMPMC in sealed glass
145 vials, in order to simulate a flooding period. Anoxic incubation of the S1 and S2 samples
146 (S1_anox_bio_1ml_t20; S2_anox_bio_1ml_t20) were carried out with ~1 g of air-stored
147 sample in 1ml of O_2-free milli-Q water in 50 ml tinted glass vials sealed with a butyl rubber
148 stopper for 20 days. Similar conditions were applied for the C2-5cm sample (C2-5

149 cm_anox_bio_1ml_t20) with ~300 mg of vacuum dry solid sample. No duplicates were
150 carried out for these anoxic incubations.
151 Additional anoxic incubations of the S1 and S2 samples were carried out in duplicate, with a
152 lower solid:liquid ratio (1:10) during 14 days (S1_anox_bio_10ml_t14_A;
153 S1_anox_bio_10ml_t14_B; S2_anox_bio_10ml_t14_A; S2_anox_bio_10ml_t14_B; A and B
154 corresponding to duplicates). Abiotic control incubations were conducted similarly but with
155 samples previously autoclaved at 120°C for 20 min (S1_anox_abio_10ml_t14;
156 S2_anox_abio_10ml_t14). For these 1:10 incubations, ~1 g of wet soil sample was
157 supplemented by 10 ml of an anoxic 9 $mg.L^{-1}$ NaCl solution, put in 50 ml tinted glass vials,
158 sealed by a butyl rubber stopper and tumbled for 14 days. For these latter experiments, NaCl
159 was used as background electrolyte in order to avoid osmotic stress of the microbial biomass.
160 At the end of these experiments, the incubation solutions were collected by centrifugation,
161 filtered through 0.2 µm and an aliquot was acidified to pH~1 using 67 % HNO_3 for further
162 dissolved U analysis.
163 At the end of all incubation experiments solid samples were vacuum dried in a desiccator
164 placed in a glove box and stored under anaerobic conditions for further analyses.
165
166 **2. 3. Chemical Analyses procedures**
167
168 The initial solid soil samples of the C2 and C6 cores were previously analyzed for majors and
169 traces elements [10]. For S1 and S2 initial solid samples, U content was measured by gamma
170 spectrometry using a Ge HP type N - GEN27 detector at IRSN laboratory. For this purpose,
171 solid samples were dried at 105 °C until a constant mass was obtained. They were 2mm
172 sieved and ~40 g of the fraction inferior to 2mm was conditioned under vacuum in aluminized
173 bag. Each sample was measured for 24 hours. Dissolved uranium in the 1:10 incubation

experiments were measured on acidified aliquots using an ICP-MS (X7 série 1 ThermoFisher®). Dissolved Organic Carbon (DOC) and Dissolved Inorganic Carbon (DIC) were measured following the method described in Stetten et al. (2018b) [10].

2. 4. X-ray Absorption Spectroscopy

X-ray Absorption Near Edge Structure (XANES) and Extended X-ray Absorption Fine Structure (EXAFS) spectra at the Uranium L_{III}-edge were collected on the 11-2 wiggler beamline at the Stanford Synchrotron Radiation Lightsource (SSRL) and on the CRG-FAME bending-magnet beamline at the European Synchrotron Radiation Facility (ESRF). The S1, S2 and anoxic incubation samples were analyzed on the 11-2 beamline at liquid N_2 temperature in fluorescence mode detection using a Si(220) double crystal monochromator and a 100-element solid state Ge array fluorescence detector. The oxic incubation samples were analyzed on the FAME beamline at liquid He temperature using a Si(220) double crystal monochromator and a 30 elements Ge fluorescence detector (ESRF) [23]. The incident beam energy was calibrated using a Y-foil in double transmission setup, with first inflection point set to E=17038 eV. XAS spectra collected at BL 11-2 were deadtime corrected and average using SIXPACK [24], and those collected at FAME-CRG beamline were averaged using ATHENA [25]. Energy calibration, normalization and background subtraction were performed with ATHENA.

In order to quantitatively determine the fractions of U(VI) and U(IV), U-L_{III} edge XANES spectra were least-squares fit by linear combinations (LCF) of pure U(IV) and U(VI) model compounds XANES spectra, using a home-built code [10,19,26]. The chosen model compounds were a U(IV) humus sample and a synthetic U(VI)-humic acid model compound [10]. Uranium L_{III}-edge EXAFS spectra of the incubated samples were least-squares fit by

linear combinations (LCF) of model compounds EXAFS spectra using a home-built code [10,19,26]. The model compounds chosen for this procedure were already used by Stetten et al. (2018b) [10] to fit the U L_{III}-edge EXAFS spectra of the C2 and C6 soil samples and were previously interpreted using shell-by-shell fitting of the k^3-EXAFS spectra. This latter procedure yielded a description of the first and second neighbor shells around the U atom in these model compounds, as detailed in Stetten et al. (2018a) [5] and Stetten et al. (2018b) [10].

2. 5. µ-XRF and µ-XAS data collection and analysis.

Microfocused X-ray fluorescence (µ-XRF) and U L_{III}-edge micro-X-ray Absorption Near Edge Structure (µ-XANES) spectroscopy analyses were conducted at the 2-3 beamline (SSRL) on polished sections of epoxy resin-embedded samples. The chosen samples were the mine water deposit sample (S2) and the product of its 20-day incubation under anoxic conditions (S2_anox_bio_1ml_t20). The µ-XRF maps were collected at room temperature and an incident energy of 17200 eV, using a Vortex silicon drift detector, a beam spot size of ~2x2 µm, a step of 10 µm and a counting time of 50ms. In order to limit U(IV) oxidation, a continuous flow of N_2 gas was applied on the surface of the samples during the measurements. Points of interest were selected on the µ-XRF maps for U L_{III}-edge µ-XANES analyses using a Si(111) monochomator calibrated with elemental Y (K-edge at 17038 eV). The spectra were averaged using SIXPACK [24], normalized with ATHENA and analyzed by LCF with a custom-built software based on Levenberg-Marquardt least-squares minimization algorithm, using U(VI)-humic acid and U(IV)-humus model compound spectra as fitting components [5,10].

2. 6. SEM-EDXS data collection and analysis

Scanning electron microscopy analyses were performed at IMPMC, using a Zeiss ultra 55 equipped with a Field Emission Gun. Backscattered images and EDX Spectra were collected at 15 keV with a working distance of 7.5 mm. The beam intensity was calibrated using the Cu K-alpha emission from a TEM copper grid. Semi-quantification of the EDXS spectra was performed using the Bruker® Esprit program and the Phi(rho,z) method using mineral standard spectra. The atomic content in U, Ca and P obtained with this method were then plotted in ternary diagrams using TERNPLOT [27].

3. RESULTS AND DISCUSSION

3. 1. Effect of oxic incubations

In the pristine wetland soil samples (C2-25 cm, C2-30 cm and C6-33 cm samples), ~40-58% U(IV) is present as mononuclear U(IV) species that were fitted with a U(IV)-humus component (Figure 1, Table SI-2). In this model compound, the U-P at 3.1 Å and U-C at 3.7 Å EXAFS scattering paths are interpreted as bidentate and monodentate binding of U to phosphate and carboxylate groups, respectively [10]. The remaining ~35-55 % U in the soil samples was fitted with a U(IV)-rhabdophane component, used as proxy for U(IV) phosphate minerals identified as ningyoite and lermontovite [10].

After 20 days of incubation under oxic conditions, the proportion of mononuclear U(IV) decreased down to 0-17% and that of U(IV)-phosphate mineral decreased down to 20-38 %, while mononuclear U(VI) increased to 51-89 %, as fitted with a U(VI)-biosorbed component (Figure 1; Table SI-2). In this latter model compound, U(VI) is bound to both phosphate in

monodentate geometry (U-P path at ~3.6 Å; [10,28,29]) and carboxylate in bidentate geometry (~2 U-C paths at 2.9 Å; [10]). These data are consistent with the extent of U oxidation measured by LCF-XANES analysis of the same samples (Figure SI-3, Table SI-2). These results indicate complete oxidation of mononuclear U(IV) (Figure 1), except for sample C2-25 cm in which 17 % of mononuclear U(IV) persisted, which is consistent with the reported higher sensitivity of mononuclear species to redox change than crystalline U(IV) species [15-18]. In addition, except in sample C2-25 cm, 30-45 % of the U(IV)-phosphate minerals oxidized, likely into U(VI)-mononuclear species that were accounted by an increase of the U(VI)-biosorbed component in the LCF. These oxidized species could correspond to mononuclear U(VI) bound to organic phosphate groups of humic substances or biomass [28,30], as well as to inorganic phosphate groups [28,33] for instance at the surface of the oxidized U(IV)-minerals. Finally, 55-100 % of the U(IV) mineral phases were resistant to oxidation. The study of Newsome et al. (2015a) [16] also highlighted that U(IV)-phosphate minerals were partly resistant to oxidation. In this previous study, only ~20 % of U(IV) was reoxidized from a biologically precipitated ningyoite-like phase after 90 days of air exposure.

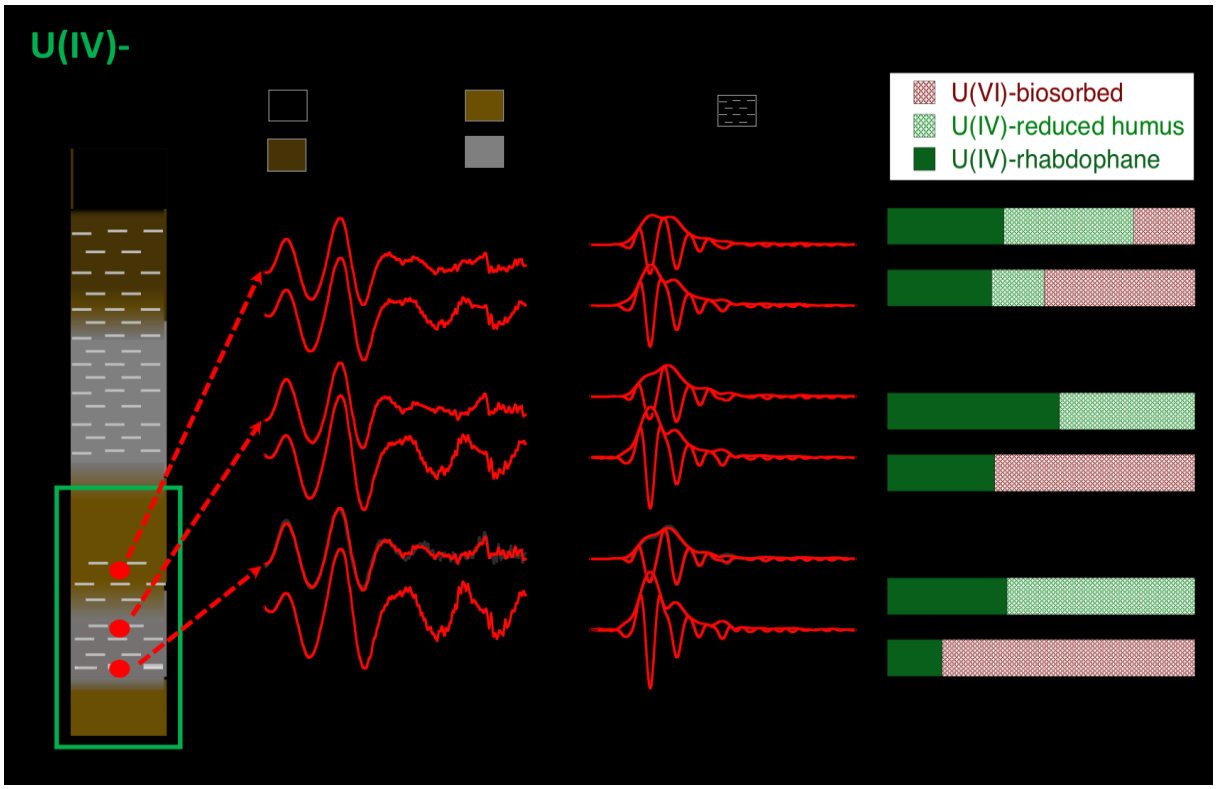

Figure 1. LCF analysis of U L_{III} EXAFS data of pristine reduced soil samples from the A_2-type and mine water deposit layers and same samples after incubation under oxic conditions. Experimental and fit curves are displayed in black and red colors respectively. Modulus and Imaginary part of the Fast Fourier Transforms of the experimental and fit curves are also reported. The proportions of the fitting components, represented by the bar-diagram, are normalized to 100 %. Non-normalized results and uncertainties are given in Table SI-2.

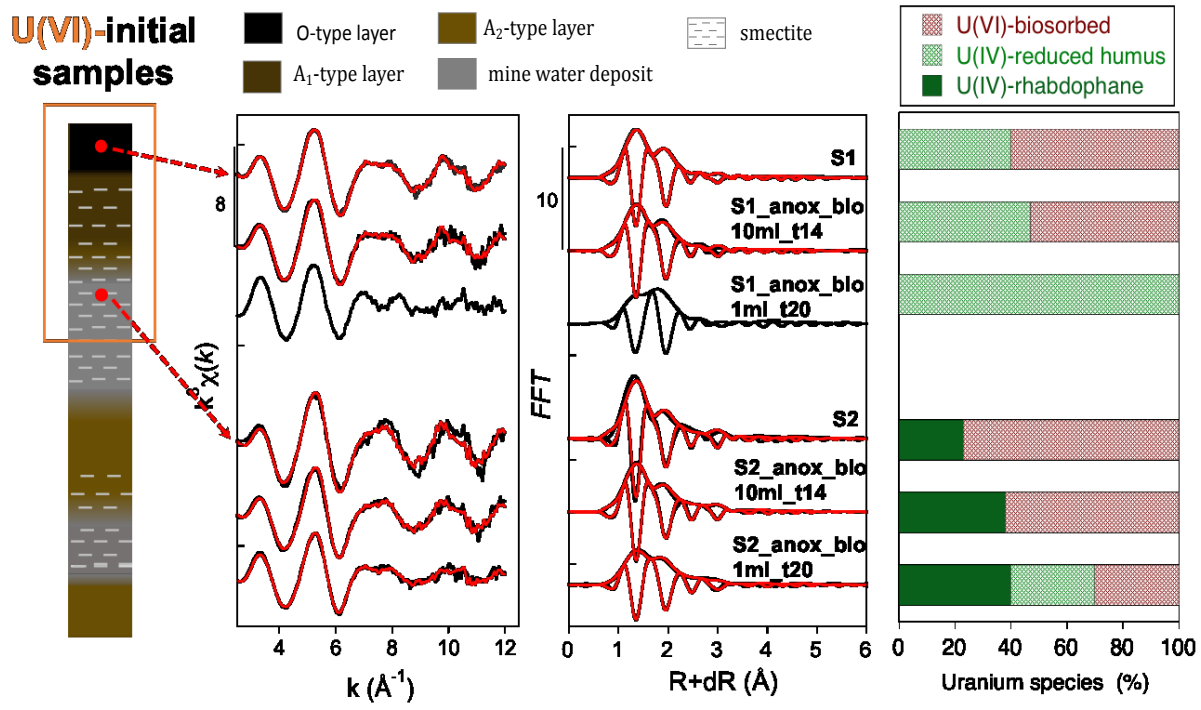

Figure 2. LCF analysis of U L_{III} EXAFS data of initial samples (S1 and S2 samples) and incubated samples under anoxic conditions. Experimental and fit curves are displayed in black and red colors respectively. Modulus and Imaginary part of the Fast Fourier Transforms of the experimental and fit curves are also reported. The proportions of the fitting components, represented by the histograms, are normalized to 100 %. Non-normalized results and uncertainties are given in Table SI-2.

In order to evaluate the consequences of the oxidation of U(IV)-mineral phases on the potential U redistribution in the soil matrix, the spatial distribution of U was investigated by µ-XRF mapping. The sample studied was a polished cut of the air dried S2 mine water deposit sample that exhibited the same U speciation as C2-30cm_oxic and C6-33 cm samples (Figures 2 and 1; Table SI-2). Uranium was mainly found by µ-XRF as hot spots (Figure 3a) suggesting the presence of U minerals grains. LCF analysis of µ-XANES spectra collected at hotspots #1 and #2 showed only U(IV) (Table SI-4). These grains could thus be interpreted as corresponding to abundant ningyoite $CaU(PO_4)_2 \cdot 2H_2O$ (Figures 4d,4a, SI-4a), and to a lesser extent lermontovite $U(PO_4)(OH) \cdot H_2O$ (Figures 4c; SI-4b) grains identified by SEM-EDXS in the same S2 sample.

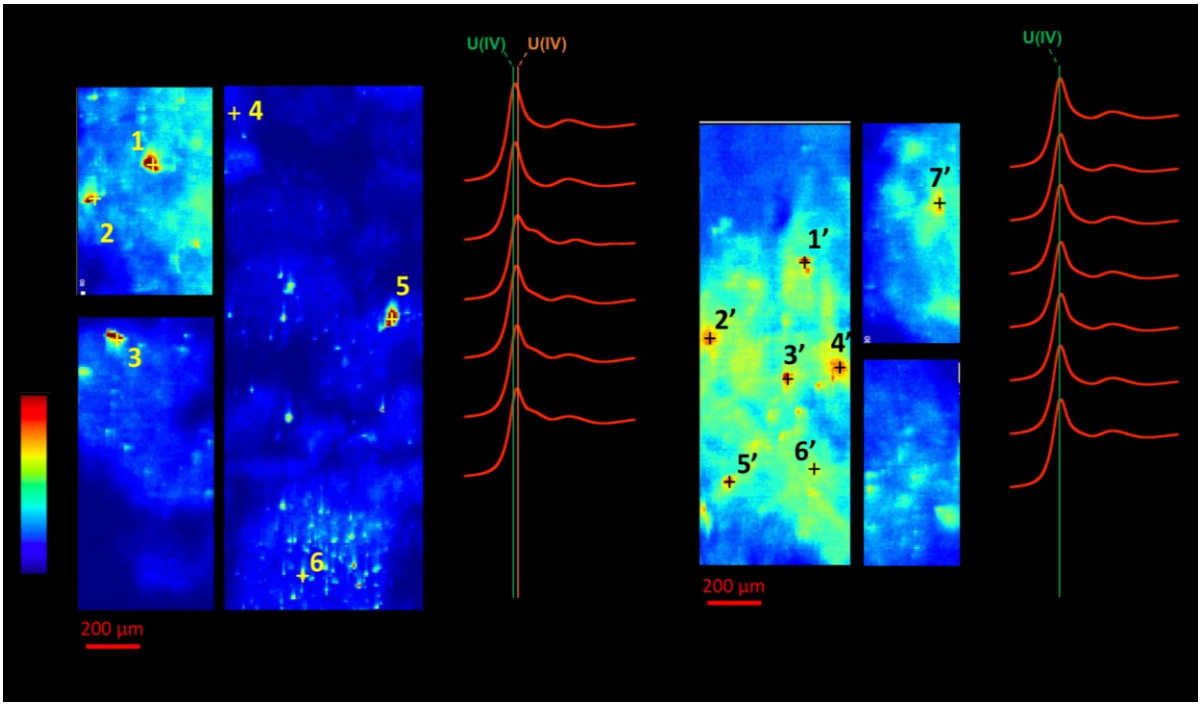

Figure 3: µ-XRF mapping of U distribution and µ-XANES analyses of U redox state in a mine water deposit sample collected in the wetland (Sample S2) and the product of its incubation under anoxic conditions (S2_anox_bio_1ml_t20); The data were obtained by analyzing polished sections of epoxy-

resin embedded samples. The μ-XRF elemental maps are displayed in the same color intensity scale and show the spreading of U around U-rich grains in the incubated sample. The color scale of the μ-XRF elemental maps corresponds to the background subtracted area of the U Lα emission line, increasing from blue to red with U content; U oxidation state was determined by LCF fit of the micro-XANES spectra collected on selected points in the XRF maps using U(VI)-humic acid and U(IV)-humus model compound spectra as fitting components. Spectrum of these model compounds are plotted in black lines. Experimental and calculated spectra are plotted as black and red solid lines, respectively. No oxidation of U(IV) was reported during the time of the measurement as shown in Figure SI-6. Non-normalized results and uncertainties are given in Table SI-4.

Spot #3 exhibited only U(VI) could be attributed to crystalline autunite $Ca(UO_2)_2(PO_4)_2 \bullet 11H_2O$ that was scarcely observed in this sample (Figure SI-4c). Since no U(VI)-bearing mineral was detected by EXAFS analysis of this sample, autunite likely do not account for more than 10 % of total U in the S2 sample. The formation of an autunite-like mineral after oxidation of an amorphous U(IV)-phosphate was reported by Latta et al. (2016) [22]. By contrast, in the mine water deposit S2 sample, the scarce and massive autunite crystals (Figure SI-4c) differs from the reticulated microcrystals observed by Latta et al. (2016) [22], and thus did not likely formed by the oxidation of ningyoite. Instead, our μ-XAS dataset and the non-detectability of U(VI)-mineral by EXAFS suggest that U(IV) minerals grains oxidized into mixed U(IV)/U(VI) grains, in which U(VI) may be mainly present as sorbed mononuclear U(VI). Indeed, the observation of U(VI) in hot spots #4, 5 and 6 suggested that these U-rich grains contain sorbed U(VI) that could coat or replace former U(IV)-phosphate phases. Finally, the μ-XRF map of the initial S2 sample (Figure 3) displayed a diffuse distribution of U, which was consistent with the occurrence of U(VI) mononuclear complexes determined by LCF-EXAFS (Figure 2; Table SI-2). Altogether, these results confirmed that a fraction of U is distributed in the soil matrix, which might account for the non-crystalline U(VI) species observed by EXAFS analysis.

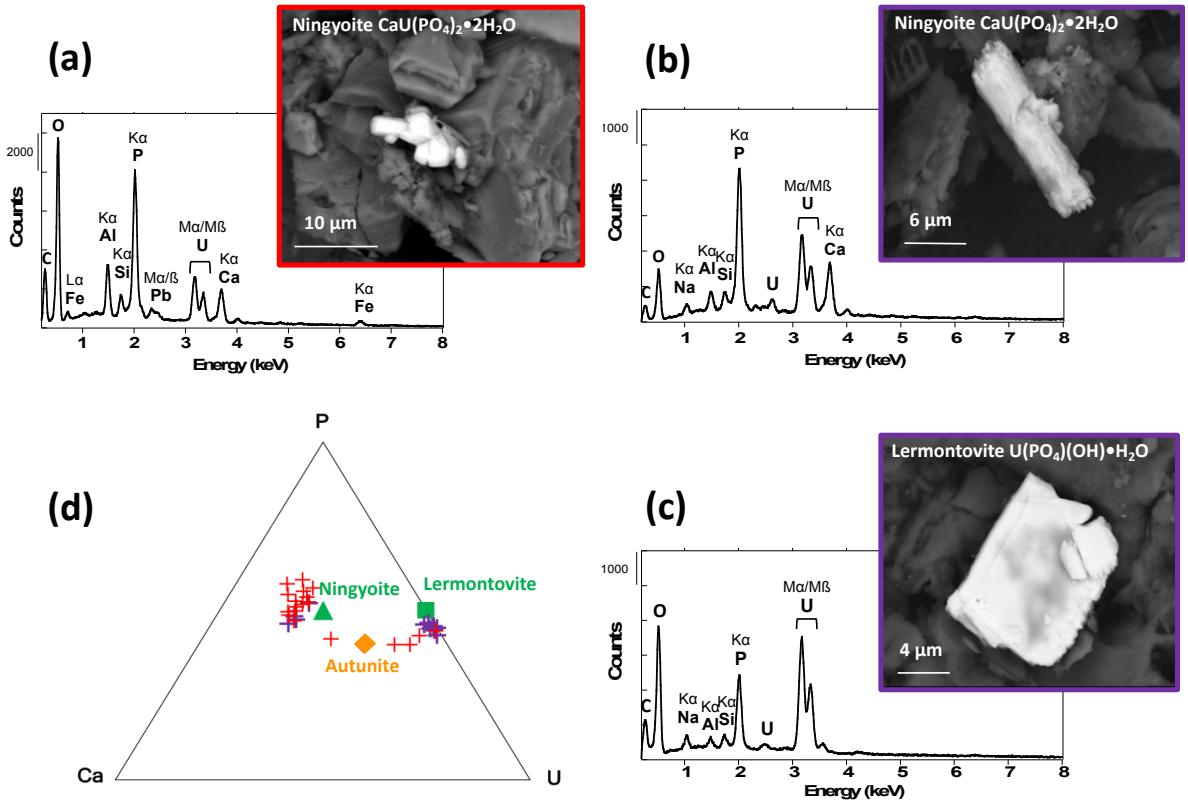

Figure 4. Backscattered electrons SEM images and semi-quantitative EDXS analyses of U minerals in the mine water deposit (S2 sample; red crosses) and in the same sample after anoxic incubation (S2_anox_bio_1ml_t20; purple crosses). (a) Ningyoite in the S2 sample, (b) Ningyoite with prismatic morphology [34] and (c) Lermontovite with platy morphology [37] in the S2_anox_bio_1ml_t20 incubated sample. (d) Ternary diagram showing P, Ca and U compositions of the U-mineral grains observed in these samples. Ideal stoichiometric composition of Autunite $Ca(UO_2)_2(PO_4)_2•11H_2O$ (orange diamond), ningyoite $CaU(PO_4)_2•2H_2O$ (green triangle) and lermontovite $U(PO_4)(OH)•H_2O$ (green square) minerals are also reported.

3. 3. Effect of anoxic incubations

Two types of samples were incubated under anoxic conditions: S1 and C2_5cm humus samples in which U mainly occurs as mononuclear species and S2 mine water deposit sample in which U is partitioned between U-phosphate minerals and mononuclear species. Full reduction of U(VI) was observed for S1 and C2_5 cm, whereas partial reduction was observed for S2 (Figures 2 and SI-3; Tables SI-2 and SI-3) after 20 days. The extent of U

342 reduction was systematically lower at shorter incubation times (14 days) and at lower
343 solid:liquid ratio (1:10) (Figure 2; Table SI-2). We may hypothesize that a lag phase in the
344 growth of the microbial biomass could have delayed the effective microbial-mediated U
345 reduction during the first 14 days of incubation. The reduction of U(VI) to U(IV) species
346 could be enhanced by both enzymatic and abiotic U(VI) reduction pathways [5, 37-40]. Here,
347 the role of microorganisms in U reduction was confirmed by the absence of U reduction in the
348 abiotic incubations conducted for 14 days at solid:liquid ratio (1:10) (Figure SI-3; Table SI-
349 3). The higher reduction rate observed for S1 samples could be explained by the high organic
350 carbon content of these samples that would have enhanced biotic reduction processes [37],
351 likely *via* direct or indirect dissimilatory reduction of U(VI) [38-40]. Even if it has been
352 shown that direct enzymatic U reduction pathways dominate in sediments [36, 39], we cannot
353 exclude that U is reduced by indirect microbial pathways, for example *via* the release of
354 abiotic reductants such as Fe(II), itself possibly produced by the bioreduction of Fe(III)-
355 bearing minerals [5, 40].
356 For the S1 sample, the best EXAFS LCF was obtained with 60% of U(VI)-biosorbed model
357 compound and 40% of U(IV)-humus model compound (Figure 2; Table SI-2). This latter
358 model compound also used by Stetten et al. (2018b) [10] corresponds to the product of
359 reduction of the S1 sample after 20 days of incubation at high solid:liquid ratio
360 (S1_anox_bio_1ml_t20 sample), in which U was fully reduced (Figures 2 and SI-3; Tables
361 SI-2 and SI-3). Shell-by-shell fitting of the k^3-EXAFS spectra was performed in Stetten et al.
362 (2018b) [10] for this humus model compound and indicated the presence of bidentate U(IV)-
363 phosphate and monodentate U(IV)-carboxylate complexes.
364 Altogether, these results suggest that the reduction of monodentate U(VI)-phosphate and
365 bidentate U(VI)-carboxylate complexes lead to the formation of bidentate U(IV)-phosphate
366 and monodentate U(IV)-carboxylate complexes, without formation of U(IV) mineral, likely

367 due to the abundance of organic-bound phosphate and carboxylate ligands inhibiting uraninite
368 formation [41,42]. Additionally, the lack of free orthophosphate may also prevent U(IV)-
369 phosphate minerals precipitation in such organic-rich layers.
370 Sample S2 was chosen to investigate the effect of anoxic conditions on oxidized mine water
371 deposits that contained mainly sorbed mononuclear U(VI) species (~80 %) and recalcitrant
372 U(IV)-phosphate minerals (~20 %) (Figures 2, 3 and 4; Table SI-2). LCF-EXAFS results
373 indicated that after 14 days of anoxic incubation (sample S2_anox_bio_10ml_t14_A), the
374 proportion of U(IV)-phosphate minerals increased up to 40% whereas sorbed mononuclear
375 U(VI) species decreased by 20 % (Figures 2; Table SI-2). After 20 days of anoxic incubation
376 (sample S2_anox_bio_1ml_t20), the proportion of U(IV) phosphate did not increase above
377 ~40 %. In contrast, the proportion of sorbed U(VI) decreased down to 31 % while a
378 proportion of ~30 % of U was found as U(IV)-humus (Figure 2, Table SI-2). This latter result
379 could be interpreted as the reduction of sorbed U(VI) to sorbed U(IV), as discussed in the
380 previous section for S1 sample.
381 The increase in the proportion of U(IV)-phosphate minerals after 14 and 20 days of anoxic
382 incubation suggests the formation of U(IV)-phosphate minerals. Such a reaction may likely
383 occur *via* reduction of U(VI) bound to phosphate mineral surfaces since the reduction of
384 organically-bound U(VI) was found to lead to organically bound U(IV) as shown for S1
385 sample. The formation of U(IV)-phosphate such as ningyoite-like minerals from the
386 bioreduction of inorganic U(VI)-phosphate species is supported by previous laboratory assays
387 [21,43]. Indeed, these previous studies reported slow reduction kinetics of Hydrated Uranium
388 Phosphate (HUP), with ~20-80 % of U(VI) remaining in the solid phase after 10 days
389 incubation of a biogenic HUP, and ~30 % of U(VI) after 20 days incubation of abiotic HUP.
390 To this regard, the lower reduction rate observed in S2 sample compared to the organic S1

sample may be due to a slower bioreduction rate of inorganic U(VI)-phosphate species compared to organic ones.

In the incubated S2_anox_bio_1ml_t20 sample, µ-XANES spectra for U(IV)/U(VI) ratio showed that a minor (10-35%) proportion of U(VI) remained at hot spots (Figure 3b; Table SI-4), suggesting almost complete reduction of U(VI)-bearing mineral grains. In addition, the amount of U in the soil matrix appeared to be higher after than before incubation (Figures 3a and 3b), suggesting U migration from U hot-spots to the surrounding organic-rich soil matrix (Figure 3b). One may hypothesize that such migration process could have occurred at the beginning of the incubation experiment *via* the dissolution of U(VI) initially sorbed to oxidized phosphate minerals grains (Figure 5). The presence of U(IV) in the soil matrix (Figure 3b; Table SI-4) suggests that U(VI) was then further reduced to U(IV) mononuclear species under the reducing conditions that developed in these anoxic incubations.

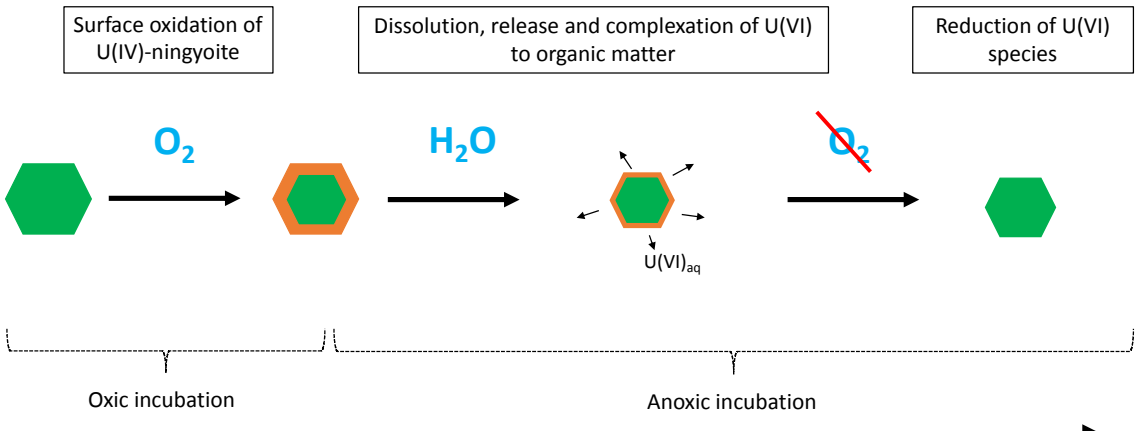

Figure 5. Schematic view of the effect of successive oxic and anoxic incubations on the redistribution of U from U(IV)-phosphate mineral such as ningyoite in mine water deposits layers in the studied contaminated wetland.

SEM-EDX observations revealed a higher amount of lermontovite-like minerals (Figures SI-5c) after anoxic incubation, *i.e.* in the S2_anox_bio_1ml_t20 sample, than in the S2 sample

412 (Figures 4d, SI-4b). Conversely, ningyoite was also found in the S2_anox_bio_1ml_t20
413 sample (Figure SI-5ab) but in a lower amount than in the S2 sample (Figures 4d, SI-4a).
414 Moreover, some ningyoite grains observed in this sample exhibited a weathered morphology
415 with acicular apexes and eroded surfaces (Figures 4b, SI-5b), whereas lermontovite grains
416 exhibited massive and non-weathered morphology (Figure 4c, SI-5c). These results suggest
417 that sorbed U(VI) previously resulting from the oxidation of ningyoite grains could have
418 dissolved at the beginning of the anoxic incubation, whereas lermontovite-like minerals may
419 be more recalcitrant to oxidation and dissolution. Moreover, we hypothesize that autunite-like
420 minerals of the S2 sample could have been transformed into lermontovite-like minerals *via* a
421 loss in Ca during the reduction process. Indeed, lermontovite is known to mainly occur as
422 secondary mineral in reducing environments and is found in intimate intergrowth with U(VI)-
423 phosphates from the autunite or meta-autunite group [35]. In addition, although the crystal
424 structure of lermontovite is still unsolved, it has been reported to crystallize in the
425 orthorhombic system and could thus have a layered structure like autunite [35], which could
426 favor transformation of autunite phase to lermontovite *via* the loss of Ca^{2+} in the interlayer
427 and reduction of U(VI) to U(IV). The scarcity of autunite in the wetland soil, while it is an
428 abundant mineral of the oxidation zone of the Ty Gallen ore (https://www.mindat.org/min-
429 433.html), and in return the abundance of lermontovite in the reduced mine water deposits
430 layers of the wetland could be explained by a progressive transformation of autunite into
431 lermontovite under prolonged reducing conditions. In contrast, the progressive oxidation and
432 dissolution of ningyoite, after repeated redox cycles could explain the redistribution of U
433 toward the organic compartment of the wetland soil. Finally, neoformation of ningyoite under
434 reducing conditions cannot be excluded since Khijniak et al. (2005) [43] reported the
435 formation of a ningyoite-like mineral after bioreduction of a meta-autunite mineral uramphite

436 $(NH_4)(UO_2)(PO_4).3H_2O$ at 65°C in a laboratory experiment with *Thermoterrabacterium*
437 *ferrireducens*.
438
439 **3.4. Uranium mobility after a redox cycle: experiment vs field investigation**
440
441 In order to investigate the release of U during a flooding event following a dry period, we
442 have measured dissolved U concentrations in 0.2 µm filtered supernatant solutions collected
443 at the end of the anoxic incubation. Figure 6 shows the dissolved uranium concentrations at
444 the end of the 1:10 incubation performed under biotic and abiotic anoxic conditions. Uranium
445 concentrations in the humus sample S1 experiments (S1_anox_biotic_10ml ([U]= 1520 $\mu g.L^{-1}$)
446 and S1_anox_abiotic_10ml ([U]= 2156 $\mu g.L^{-1}$)) are far higher than U concentrations of the
447 mine water deposit layer sample S2 experiments (S2_anox_biotic_10ml ([U]=160 $\mu g.L^{-1}$) and
448 S2_anox_abiotic_10ml ([U]=913 $\mu g.L^{-1}$)). Such high concentrations represented however less
449 than 0.05 % of both S1 and S2 solid U concentrations (4516 $mg.kg^{-1}$ for S1 and 2750 $mg.kg^{-1}$
450 for S2). These results showed that, in the conditions of our experiments, the remobilization of
451 U in the aqueous media after a complete redox cycle is limited and did not exceed 0.05 % of
452 the total U solid pool. Despite that the aqueous environments established in the experiments
453 are simplified, these results were consistent with our previously developed hypothesis of the
454 redistribution and scavenging of U in the solid phase during the incubation experiment,
455 mostly by adsorption and subsequent reduction (Figure 3a). These results agree with a recent
456 study showing a release of U of 0.8% from initially reoxidized mononuclear U species under
457 reducing conditions in carbonate-free media [18].
458 In all anoxic incubations, dissolved organic carbon release was high, especially for organic S1
459 samples (Table SI-5) and was positively correlated to dissolved U concentration, which
460 strongly suggests solubilization of U by complexation to soluble organic ligands. Such results

461 are in line with the study of Grybos et al. (2009) [44], in which large quantities of dissolved
462 organic matter were reported to be solubilized under reducing conditions in a wetland soil,
463 likely because of the reductive dissolution of ferric iron oxides involved in the stabilization of
464 organic matter. Organic species have been shown to complex U(VI) and U(IV) in aqueous or
465 colloidal mobile species in the laboratory and the field [7,45-46]. In the study of Seder-
466 Colomina et al. (2018) [18], U release under anoxic condition was mainly explained by
467 inorganic carbon complexation except in experiments without added HCO_3^-, where a minor U
468 mobilization was explained by the release of organic carbon. In addition, in the same study,
469 geochemical modeling confirms the presence of dissolved U(VI) and U(IV) organic species as
470 major species in the aqueous media in carbonate-free experiments. In our experiments, DIC
471 was found negligible to the opposite of DOC. In addition, EXAFS results show an important
472 fraction of U bound to organic moieties (Figure 2) in the solid phase. The final dissolved U in
473 all our incubated samples could therefore be associated with soluble or colloidal forms of
474 organic carbon. Then, for the S1 sample, the release of U could be due to the release of U-
475 bearing organic molecules. For the S2 sample, the dissolution of U(VI)-phosphate minerals
476 could be more limited because of the lower amount of organic carbon, but still promoted by
477 complexation to soluble organic ligands. Accordingly, laboratory experiment have reported
478 important remobilization of U after reoxydation of non crystalline U(IV) [15]. In contrast,
479 U(IV)-phosphate minerals were found to be more recalcitrant to oxidative remobilisation, but
480 significant release of U was also reported [16]. Here, our results suggested that such
481 remobilization could be limited in organic-rich environmental samples, *via* U sorption onto
482 particulate matter. Indeed, uranium remobilization was found to be minor (< 1% of total solid
483 U). However, the high concentrations of U in the soil (< 4500 $mg.kg^{-1}$) could contribute to
484 significant dissolved U concentrations in pore waters under reducing condition. Moreover, the
485 presence of U(IV)-phosphate minerals that are subject to reoxidation events and subsequent

dissolution appears to play an important role in the long-term release of U under redox fluctuations, even in the absence of carbonates. In addition, mobility of U bound to particulate and colloidal organic matter would be important to consider in order to evaluate U fluxes out of the studied wetland.

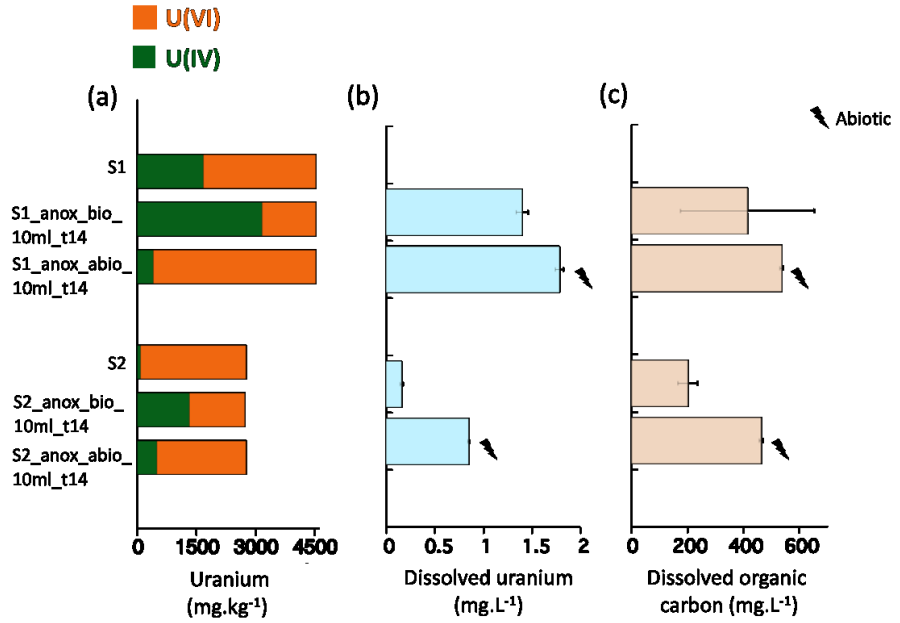

Figure 6. (a) Uranium concentration and redox in S1, S1_anox_bio_10ml_t14, S1_anox_abio_10ml_t14 and S2, S2_anox_bio_10ml_t14_A and S2_anox_abio_10ml_t14 solid samples. (b) U concentration in biotic and abiotic incubation solutions of S1_anox and S2_anox incubated samples at the end of the 14 days (c) Dissolved organic carbon concentrations in biotic and abiotic incubation solutions of S1_anox and S2_anox incubated samples at the end of the 14 days. Corresponding data are reported in Table SI-5. Errors bars represent the standard deviation over the duplicates samples for biotic incubations and the relative uncertainty of the measurement for abiotic incubations.

4. CONCLUSION

In our previous study of the same wetland, we showed an important redistribution of U from U(IV)-phosphates to mononuclear U(VI)/U(IV) species, interpreted as the result of the oxidative dissolution of U-phosphate minerals and subsequent adsorption of U by organic matter occuring during redox oscillations [10]. Here, our results confirm that a drying period could enhance rapid oxidation of non crystalline species and, to a lesser extent, of U(IV)-

phosphate minerals. Even if such oxidation has been shown to lead to an important remobilization of U, especially if it is under non-crystalline forms [15-16], our results show that in organic-rich samples, the adsorption onto soil organic ligands limits U spreading from mineral hotspots. In addition, the dissolution of U(IV)-phosphate minerals upon redox cycling raises important issues concerning the long-term fate of U in seasonnaly saturated environments. Our results further suggest that mononuclear U(VI) species resulting from such oxidative dissolution processes can be fully reduced after 20 days under reducing condition. Thus, in organic-rich and carbonate-free environments, U mobility appears to be mainly controlled by the fate of organic matter rather than by redox processes [7,47], which is supported by the observed positive correlation between aqueous U and DOC content in our anoxic incubation solutions. This observation raises questions concerning the long-term fate of U in highly contaminated organic-rich wetlands, since U could be slowly mobilized under both oxic and reducing conditions. As a perspective of this work, we hope that the molecular scale processes identified in this study will help to design efficient monitoring and modeling approaches to manage U migration at the landscape scale in organic-rich environments.

ACKNOWLEDGEMENTS

This study was conducted within the framework of the IRSN/IMPMC collaborative research program number LS 20218/C151903-P150778. The authors thank Jean-Louis Hazemann and Olivier Proux for their help on the FAME-CRG beamline (ESRF) and Samuel M. Webb and Ryan Davis for their help during measurements at the 2-3 and 11-2 SSRL beamlines respectively. Portion of this research was carried out at the Stanford Synchrotron Radiation Light Source, a national user facility operated by Stanford University, and behalf of the US DOE Office of Basic Energy Sciences. Jean-Claude Boulliard is greatly acknowledged for having supplied mineral species samples from the IMPMC mineralogy collection. The SEM-

532 EDXS and XRD platforms of IMPMC are also acknowledged for having provided time for
533 analyses. The anonymous owner of the site is also acknowledged for giving us access to the
534 site. Lucie Stetten's PhD has been granted by Region Ile de France, DIM R2DS PhD grant
535 number 2015-03.

REFERENCES

[1] D. Brugge, J.L. De Lemos, B. Oldmixon, Exposure Pathways and Health Effects Associated with Chemical and Radiological Toxicity of Natural Uranium: A Review, Reviews on environmental health 20 (2005).

[2] S.R. Taylor, Abondance of chemical elements in the continental crust: a new table, Geochim. Cosmochim. Acta 28 (1964) 1273-1285.

[3] M. Cuney, The extreme diversity of uranium deposits, Miner Deposita 44 (2009) 3–9.

[4] K.M. Campbell, R.K. Kukkadapu, N.P. Qafoku, A.D. Peacock, E. Lesher, K. H. Williams, J.R. Bargar, M.J. Wilkins, L. Figueroa, J. Ranville, J.A. Davis, P. E. Long, Geochemical, mineralogical and microbiological characteristics of sediment from a naturally reduced zone in a uranium-contaminated aquifer, Applied Geochemistry 27 (2012) 1499–1511.

[5] L. Stetten, A. Mangeret, J. Brest, M. Seder-Colomina, P. Le Pape, M. Ikogou, N. Zeyen, A. Thouvenot, A. Julien, G. Alcalde, J.-L. Reyss, B. Bombled, C. Rabouille, L. Olivi, O. Proux, C. Cazala, G. Morin, Geochemical control on the reduction of U(VI) to mononuclear U(IV) species in a contaminated lake sediment, Geochim. Cosmochim. Acta 222 (2018a) 171-186.

[6] A. Cuvier, L. Pourcelot, A. Probst, J. Prunier, G. Le Roux, Trace elements and Pb isotopes in soils and sediments impacted by uranium mining, Science of the Total Environment 566–567 (2016) 238–249.

[7] Y. Wang, M. Frutschi, E. Suvorova, V. Phrommavanh, M. Descostes, A. A. A. Osman, G. Geipel, R. Bernier-Latmani, Mobile uranium(IV)-bearing colloids in a mining impacted wetland, Nature Geosciences 4:2942 (2013). doi: 10.1038/ncomms3942.

[8] Y. Wang, A. Bagnoud, E. Suvorova, E. McGivney, L. Chesaux, V. Phrommavanh, M. Descostes, R. Bernier-Latmani, Geochemical control on uranium(IV) mobility in a mining-impacted wetland, Environ. Sci. Technol. 48 (2014) 10062−10070.

571 [9] A. Mangeret, P. Blanchart, G. Alcalde, X. Amet, C. Cazala, M.O. Gallerand, An evidence
572 of chemically and physically mediated migration of 238U and its daughter isotopes in the
573 vicinity of a former uranium mine, Journal of Environmental Radioactivity 195 (2018) 67-71.
574
575 [10] L. Stetten, P. Banchart, A. Mangeret, P. Lefebvre, P. Le Pape, J. Brest, P. Merrot, A.
576 Julien, O. Proux, S.M. Webb, J. R. Bargar, C. Cazala, G. Morin, Redox fluctuations and
577 organic complexation govern uranium redistribution from U(IV)-phosphate minerals in a
578 mining-polluted wetland soil, Brittany, France, Environ. Sci. Technol. 52(22) (2018b) 13099-
579 13109.
580
581 [11] A. Schöner, C. Noubactep, G. Büchel, M. Sauter, Geochemistry of natural wetlands in
582 former uranium milling sites (eastern Germany) and implications for uranium retention,
583 Chemie der Erde 69 (2009) 91–107.
584
585 [12] C. Mikutta, P. Langner, J.R. Bargar, R. Kretzschmar, Tetra- and Hexavalent uranium
586 forms bidendate- mononuclear complexes with particulate organic matter in a naturally
587 uranium- enriched peatland, Environ. Sci. Technol. 50 (2016) 10465-10475.
588
589 [13] D. Li, D.I. Kaplan, H.-S. Chang, J.C. Seaman, P.R. Jaffé, P. Koster van Groos, K.G.
590 Scheckel, C.U. Segre, N. Chen, D.-T. Jiang, Spectroscopic evidence of uranium
591 immobilization in acidic wetlands by natural organic matter and plant roots, Environ. Sci.
592 Technol. 49 (2015) 2823−2832.
593
594 [14] D.S. Alessi, B. Uster, H. Veeramani, E.I. Suvorova, J.S. Lezama-Pacheco, J.E. Stubbs,
595 J.R. Bargar, R. Bernier-Latmani, Quantitative Separation of Monomeric U(IV) from UO2 in
596 Products of U(VI) Reduction, Environ. Sci. Technol. 46 (2012) 6150–6157.
597 https://doi.org/10.1021/es204123z.
598
599 [15] J.M. Cerrato, M.N. Ashner, D.S. Alessi, J.S. Lezama-Pacheco, R. Bernier-Latmani, J.R.
600 Bargar, D.E. Giammar, Relative reactivity of biogenic and chemogenic uraninite and biogenic
601 noncrystalline U(IV), Environ. Sci. Technol. 47 (2013) 9756-9763.
602
603 [16] L. Newsome, K. Morris, D. Trivedi, A. Bewsher, J.R. Lloyd, Biostimulation by
604 Glycerol Phosphate to Precipitate Recalcitrant Uranium(IV) Phosphate, Environ. Sci.
605 Technol. 49 (2015a) 11070-11078.

606
607 [17] L. Newsome, K. Morris, S. Shaw, D. Trivedi, J.R. Lloyd, The stability of microbially
608 reduced U(IV): impact of residual electron donor and sediment ageing, Chemical Geology
609 409 (2015b) 125–135.
610
611 [18] M. Seder-Colomina, A. Mangeret, L. Stetten, P. Merrot, O. Diez, A. Julien, E. Barker, A.
612 Thouvenot, J. Bargar, C. Cazala, G. Morin, Carbonate facilitated mobilization of uranium
613 from lacustrine sediments under anoxic conditions, Environmental Science & Technology 52
614 (2018) 9615-9624.
615
616 [19] G. Morin, A. Mangeret, G. Othmane, L. Stetten, M. Seder-Colomina, J. Brest, G. Ona-
617 Nguema, S. Bassot, C. Courbet, J. Guillevic, A. Thouvenot, O. Mathon, O. Proux, J.R.
618 Bargar, Mononuclear U(IV) complexes and ningyoite as major uranium species in lake
619 sediments, Geochemical Perspectives Letters 2 (2016) 95-105.
620
621 [20] R. Bernier-Latmani, H. Veeramani, E.D. Vecchia, P. Junier, J.S. Lezama-Pacheco, E.I.
622 Suvorova, J.O. Sharp, N.S. Wigginton, J.R. Bargar, Non-uraninite products of microbial
623 U(VI) reduction, Environ. Sci. Technol. 44 (2010) 9456-9462.
624
625 [21] X. Rui, M. J. Kwon, E.J. O'Loughlin, S. Dunham-Cheatham, J.B. Fein, B. Bunker, K.M.
626 Kemner, M.I. Boyanov, Bioreduction of Hydrogen Uranyl Phosphate: Mechanisms and U(IV)
627 Products, Environ. Sci. Technol. 47 (2013) 5668-5678.
628
629 [22] D.E. Latta, K.M. Kemner, B. Mishra, M.I. Boyanov, Effects of calcium and phosphate
630 on uranium(IV) oxidation: Comparison between nanoparticulate uraninite and amorphous
631 UIV– phosphate, Geochim. Cosmochim. Acta 174 (2016) 122-142.
632
633 [23] O. Proux, X. Biquard, E. Lahera, J.-J. Menthonnex, A. Prat, O. Ulrich, Y. Soldo, P.
634 Trévisson, G. Kapoujvan, G. Perroux, P. Taunier, D. Grand, P. Jeantet, M. Deleglise, J.-P.
635 Roux, J.-L. Hazemann, FAME: a new beamline for X-ray absorption investigations of very-
636 diluted systems of environmental, material and biological interests, Phys. Scripta 115 (2005)
637 970-973.
638
639 [24] S.M. Webb, SIXpack: a graphical user interface for XAS analysis using IFEFFIT, Phys.
640 Scr. T115 (2005) 1011−1014.
641

642 [25] B. Ravel, M. Newville, ATHENA, ARTEMIS, HEPHAESTUS: data analysis for X-ray
643 absorption spectroscopy using IFEFFIT, J. Synchrotron Radiat. 12 (2005) 537−541.
644
645 [26] G. Morin, V. Noël, N. Menguy, J. Brest, B. Baptiste, M. Tharaud, G. Ona-Nguema, M.
646 Ikogou, E. Viollier, F. Juillot, Nickel accelerates pyrite nucleation at ambient temperature,
647 Geochemical Perspectives Letters 5 (2017) 6-11.
648
649 [27] D. Marshall, Ternplot: An excel spreadsheet for ternary diagrams, Computers
650 Geosciences 22 (1996) 697–699. https://doi.org/10.1016/0098-3004(96)00012-X.
651
652 [28] M. Seder-Colomina, G. Morin, J. Brest, G. Ona-Nguema, N. Gordien, J.-J. Pernelle, D.
653 Banerjee, O. Mathon, G. Esposito, E.D. Van Hullebusch, Uranium(VI) Scavenging by
654 Amorphous Iron Phosphate Encrusting Sphaerotilus natans Filaments, Environ. Sci. Technol.
655 49 (2015) 14065−14075.
656
657 [29] S. Kelly, K. Kemner, J. Fein, D. Fowle, M. Boyanov, B. Bunker, N. Yee, X-ray
658 absorption fine structure determination of pH-dependent U-bacterial cell wall interactions,
659 Geochimica et Cosmochimica Acta 66 (2002) 3855–3871. https://doi.org/10.1016/S0016-
660 7037(02)00947-X.
661
662 [30] J.O. Sharp, J.S. Lezama-Pacheco, E.J. Schofield, P. Junier, K.-U. Ulrich, S. Chinni, H.
663 Veeramani, C. Margot-Roquier, S.M. Webb, B.M. Tebo, D.E. Giammar, J.R. Bargar, R.
664 Bernier- Latmani, Uranium speciation and stability after reductive immobilization in aquifer
665 sediments, Geochim. Cosmochim. Acta. 75 (2011) 6497–6510.
666
667 [31] H.S. Moon, J. Komlos, P.R. Jaffé, Uranium reoxidation in previously bioreduced sed-
668 iment by dissolved oxygen and nitrate, Environ. Sci. Technol. 41 (2007) 4587–4592.
669
670 [32] S.D. Kelly, Uranium chemistry in soils and sediments, in: B. Singh, M. Grafe̋ (Eds.),
671 Dev. Psychiatry, 2010, Vol. 34, pp. 411.
672
673 [33] A. Singh, J.G. Catalano, K.U. Ulrich, D.E. Giammar, Molecular-Scale Structure of
674 Uranium(VI) Immobilized with Goethite and Phosphate, Environ. Sci. Technol. 46 (2012)
675 6594−6603.
676

[34] T. Muto, R. Meyrowitz, A. M. Pommer, T. Murano, Ningyoite, a new uranous phosphate mineral from Japan, Am. Mineral. 44 (1959) 633−650.

[35] S.V. Krivovichev, J. Plášil, Mineralogy and Crystallography of Uranium, in: P.C. Burns, G.E. Sigmon (Eds.), Uranium: From Cradle to Grave, Mineralogical Association of Canada Short Courses, 2013, pp 15-119

[36] G.T.W. Law, A. Geissler, I.T. Burke, F.R. Livens, J.R. Lloyd, J.M. McBeth, K. Morris, Uranium Redox Cycling in Sediment and Biomineral Systems, Geomicrobiology Journal 28 (2011) 497–506, https://doi.org/10.1080/01490451.2010.512033.

[37] B. Gu, J. Chen, Enhanced microbial reduction of Cr(VI) and U(VI) by different natural organic matter fractions, Geochimica et Cosmochimica Acta 67 (2003) 3575–3582, https://doi.org/10.1016/S0016-7037(03)00162-5.

[38] D.R. Lovley, E.J.P. Phillips, Y.A. Gorby, E.R. Landa, Microbial reduction of uranium, Nature 350 (1991) 413−416.

[39] Y. Suzuki, S.D. Kelly, K.A. Kemner, J.F. Banfield, Direct microbial reduction and subsequent preservation of uranium in natural near-surface sediment, Appl. Environ. Microbiol. 71 (2005) 1790−1797.

[40] T. Behrends, P. Van Cappellen, Competition between enzymatic and abiotic reduction of uranium(VI) under iron reducing conditions. Chem Geol 220 (2005) 315–327.

[41] M.I. Boyanov, K.E. Fletcher, M.J. Kwon, X. Rui, E.J. O'Loughlin, F.E. Löffler, K.M. Kemner, Solution and microbial controls on the formation of reduced U(IV) phases, Environ. Sci. Technol. 45 (2011) 8336−8344.

[42] D.S. Alessi, J.S. Lezama-Pacheco, J.E. Stubbs, M. Janousch, J.R. Bargar, P. Persson, R. Bernier-Latmani, The product of microbial uranium reduction includes multiple species with U(IV)–phosphate coordination, Geochim. Cosmochim. Acta 131 (2014) 115-127.

[43] T.V. Khijniak, A.I. Slobodkin, V. Coker, J.C. Renshaw, F.R. Livens, E.A. Bonch-Osmolovskaya, N.-K. Birkeland, N.N. Medvedeva-Lyalikova, J. R. Lloyd, Reduction of Uranium(VI) Phosphate during Growth of the Thermophilic Bacterium *Thermo-*

712 *terrabacterium ferrireducens*, Applied and environmental microbiology 71 (2005)
713 6423−6426.
714
715 [44] M. Grybos, M. Davranche, G. Gruau, P. Petitjean, M. Pédrot, Increasing pH drives
716 organic matter solubilization from wetland soils under reducing conditions, Geoderma 154
717 (2009) 13-19.
718
719 [45] P. Warwick, N. Evans, A. Hall, G. Walker, E. Steigleder, Stability constants of U(VI)
720 and U(IV)-humic acid complexes, J. Radioanal. Nucl. Chem. 266 (2005) 179-190.
721
722 [46] S.E. Bone, J.J. Dynes, J. Cliff, J.R. Bargar, Uranium(IV) adsorption by natural organic
723 matter in anoxic sediments, Proc. Natl. Acad. Sci. U. S. A. 114 (2017) 711−716.
724
725 [47] M.Grybos, M.Davranche, G. Gruau, P. Petitjean, Is trace metal release in wetland soils
726 controlled by organic matter mobility or Fe-oxyhydroxides reduction?, Journal of Colloid and
727 Interface Science 314, (2007) 490–501. https://doi.org/10.1016/j.jcis.2007.04.062.
728